COMET-Project Rail4Future
**Resilient Digital Railway Systems to enhance performance**

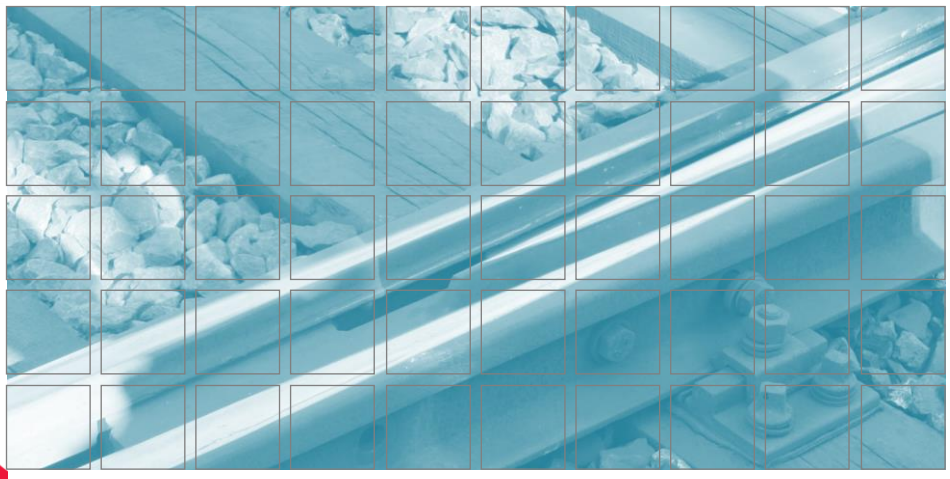

# D2.1.1 Report on Sub-Model Development

15.05.2023


Stephan Scheriau
Stephan.Scheriau@voestalpine.com

Kamil Sazgetdinov
Alexander Meierhofer
Gabor Müller
Markus Januschewsky
Georg Prinz

Roman Weilguny
Peter Brunnhofer


| | |
|---|---|
| finalized | 29.05.2023 |
| checked | 02.06.2023 |
| approved | 22.06.2023 |

# Table of content

# Preface

Components of the railway system such as rails, sleepers, ballast, switches and crossings etc. are exposed to a multitude of environmental and operational influences. The cyclic loading of rails results not only in a continuous track settlement by transferring the loads from the rail down to the sleeper and the ballast but also lead to wear and rolling contact fatigue (RCF) on rails and wheels. To describe the behaviour of the track superstructure several complex mechanisms are acting in parallel and have to be understood in detail.

The degradation of single components can be described by physical models which are implemented in multi-body dynamics, finite element or discrete element codes. A validated physical model can be used to predict the degradation of a component for a given mix of load situations. When the characteristics of the component are changed, e.g. harder rail material, the physical model is able to describe the change in the degradation curve in less rail wear, higher profile stability and less rail maintenance costs.

In this project a semi-physical plasticity model is developed to describe the wear and profile evolution on a crossing nose. The methodology captures the load situation and the hardening behaviour of the material which allows a fast calculation of the degradation behaviour of this critical crossing component. To describe wear and RCF on rails a hybrid simulation methodology is developed to predict the damage evolution in a single curve or a total track network. Data such as measured rail profiles, measured wheel profiles, rail types, actual vehicle mix and operational loads are input parameters for the model.
The interactions between track components and vehicles are described in a multibody track model that is used in different track sections such as curves, tangent tracks or on different superstructures. By changing the characteristics of single components, the vehicle-track behaviour can be studied in detail. For the optimization of the wheel-rail contact conditions a model based on DEM is developed to understand the influence of rail-roughness on the crack initiation behaviour in the rail surface.

When considering only single components or sub-systems the developed models may lead to non-optimal results for the overall railway system. Therefore, validated physical models considering the vehicle-track interaction together with environmental and operational conditions can be used for optimization of components or sub-systems to increase reliability in the railway system.

# 1 Modelling plasticity in railway turnout crossings

## 1.1 Methodology

The SPP model developed within the project is focusing on the rail profile evolution in the crossing nose region (one of the most loaded areas in railway turnouts) caused by plastic deformation. This phenomenon is dominating during the initial phase after installing a new crossing nose or after maintaining it. The development of the SPP model is based on a dataset generated with the full FEM based approach used in [1].

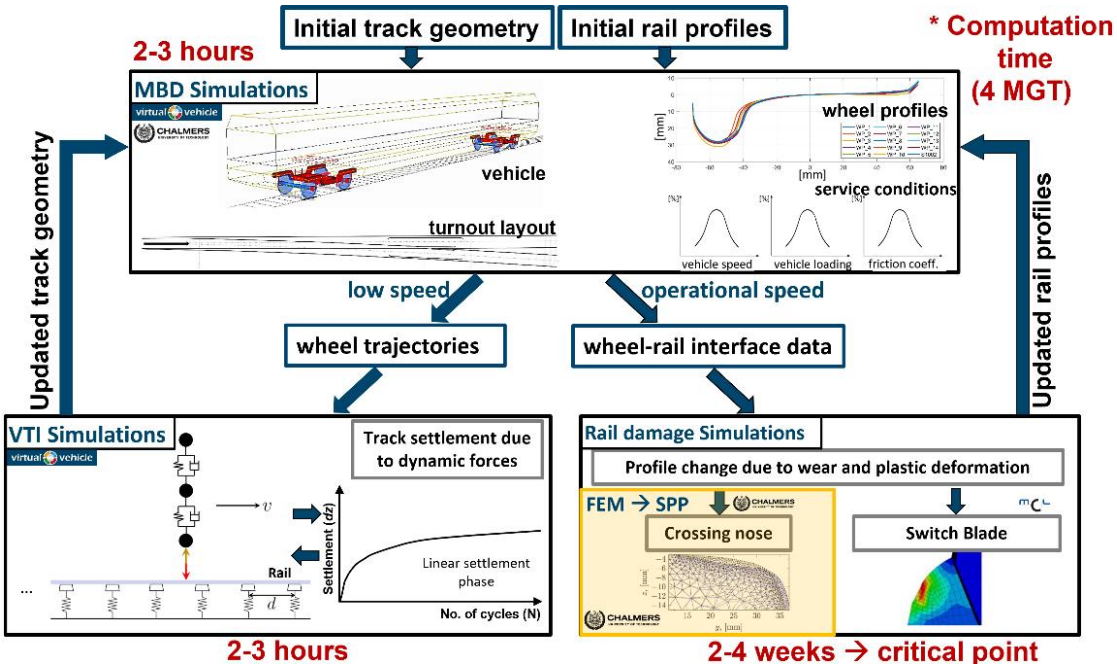


Figure 1: Whole system model-based methodology for track damage predictions in railway turnouts [1].

The operation of the SPP model – embedded into the framework shown in Figure 1 – starts with multi-body dynamics (MBD) simulations in Simpack environment with a full-scale vehicle model parametrized based on the Manchester Benchmark Vehicle [6], a commonly used turnout layout [7] and a set of measured wheel profiles [8] (representing different wear conditions) to account for realistic track operating conditions. This parametrized MBD model is used to generate wheel-rail contact interface data (input to the lower right block in Figure 1) in the region of the crossing nose (such as maximum Hertzian contact pressure, contact patch dimensions, creepages, etc.). This wheel-rail contact data is then used as an input by the SPP model to perform two types of computations (two steps):

1. Calculation of the rail profile shape change area caused by plastic deformation (see Figure 2a and b). This calculation is based on analyses of the detailed FEM dataset

generated for the rail material R350HT in combination with the MBD simulation results. This initial FEM dataset is required to calibrate the SPP model. In Figure 2a the development of the profile shape change area over traffic load (mega-gross tonnes: MGT) calculated from the FEM results is shown for three cross-sections. As expected, at the beginning a fast increase can be observed followed by a typical shake-down behaviour caused by material work hardening and reduction of contact stresses due to changed rail profile shapes.

2. Rail profile shape calculations defining where on the rail profiles along the track the calculated shape change area values must be applied and how the shapes of the rail profiles look like after a certain traffic load increment (see Figure 2b). This is based again on analyses of the detailed FEM dataset in combination with the MBD simulation results.

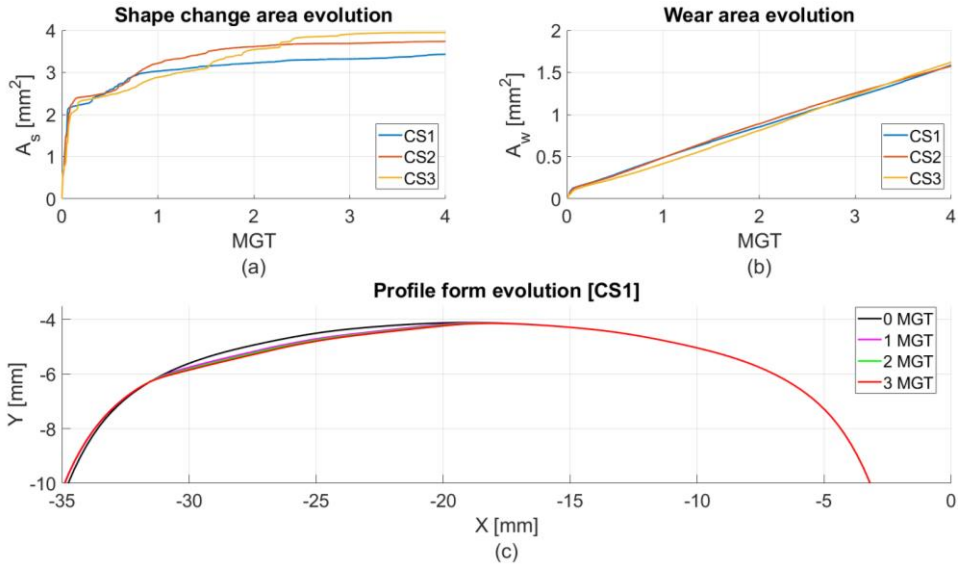


Figure 2: (a) Rail profile shape change area evolution, (b) Wear area evolution and (c) profile form evolution (CS1) calculated using the FEM dataset.

Plastic deformation in the crossing nose region is found to be mainly driven by the extremely high contact normal stresses. Therefore, in a first approach, it is assumed that for a given traffic load increment (ΔMGT) a relationship between mean maximum contact pressure (p0m) and the increment of the shape change area (ΔAs) exists, see Figure 3a.

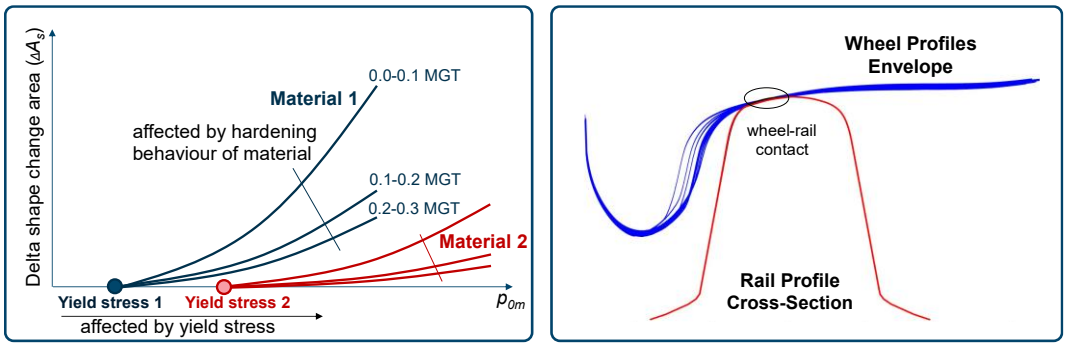


(a) (b)

Figure 3: Semi-physical plasticity (SPP) model. (a) hypothesis of the material behaviour for two rail steel grades; (b) hypothesis of the accumulative wheel profiles envelope effect on the rail profile shape evolution.

In the Figure 3, the expected influence of the yield stress and the work hardening behaviour of the rail material is indicated.

If this hypothesis is true, shape change area increments can be easily and fast calculated based on the MBD simulation results (see step 1 above). After calculating the shape change area increments along the track, the rail profile shapes need to be accordingly modified (see step 2 above). Here, the main idea is that the rail profile shapes are determined by the wheel profiles collective at a given time (resulting profiles envelope taken from MBD simulations), see Figure 3b.

## 1.2 Results

Here, first results regarding the validation of the hypotheses described above are presented. In Figure 4a depicted points show the relationship between the shape change area increments (calculated from the FEM dataset) and the mean maximum Hertzian contact pressure. Each point represents one cross-section and the corresponding mean maximum Hertzian pressure at this cross-section calculated for the different wheel profiles used in the MBD simulations at this cross-section. The results show overall a good correlation between shape change area increments and the mean maximum Hertzian pressure according to the first hypothesis, see Figure 3a. Furthermore, the dependency on the load history behaves as expected.

The second important aspect of the new methodology is the prediction of the rail profile shape at a given traffic load (MGT). Our approach proposes that the shape at a given position develops as an accumulative effect of the wheel profiles envelope taken from the

MBD simulations. In other words, at each time step (traffic load) the shapes of the rail profiles need to have the same shapes as the envelopes of the wheel profiles passing the turnout. For determining these wheel profile envelopes, the relative position and orientation of each individual wheel with respect to the rail needs to be taken into account. This information is included in the MBD simulation results. In Figure 4b exemplary results are depicted for a selected cross-section which confirms the hypothesis. The black curve shows the initial rail profile form whereas the red curve shows the evolved rail profile after 3MGT of the traffic load calculated with the full FEM approach within the framework shown in Figure 1. The blue curves show the history of the wheel profiles during the MBD simulations. The wheel profile envelope from the last simulation/time step is in good agreement with the shape of the rail profile at this step (red rail profile).

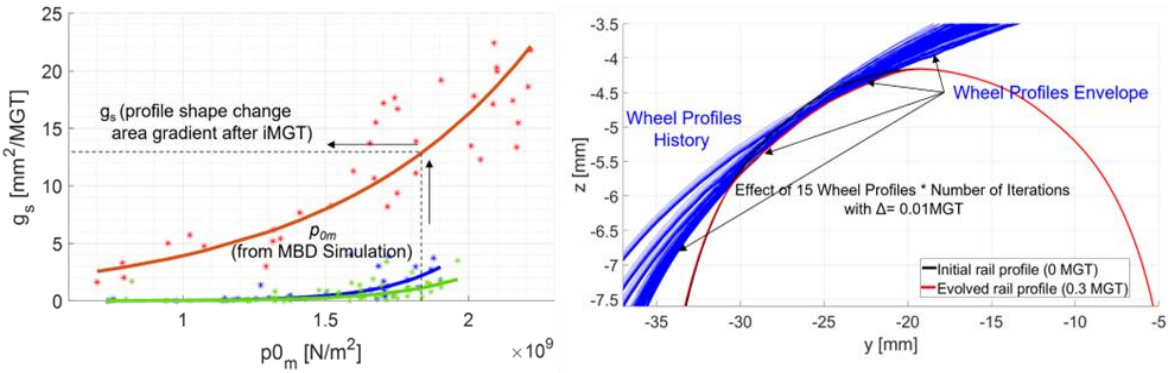


(a) (b)

Figure 4: Calculation results. (a) correlation between mean Hertzian contact stresses ($p_{0m}$) from MBD simulations and profile change area increment ($\Delta A_s$) from FEM simulations, (b) rail profile form determination as a result of the accumulative wheel profile collective effect.

A combination of the established SPP model with the accumulated effect of the wheel profiles (profile envelope) will result in a calculation time-efficient prediction of the rail profile changes in the crossing region caused by material plasticity effects.

Comparison of the SPP Model against the FEM simulation results in regard to the rail profile shape change are shows relatively good agreement in different cross-section levels as shown in the Figure 5.

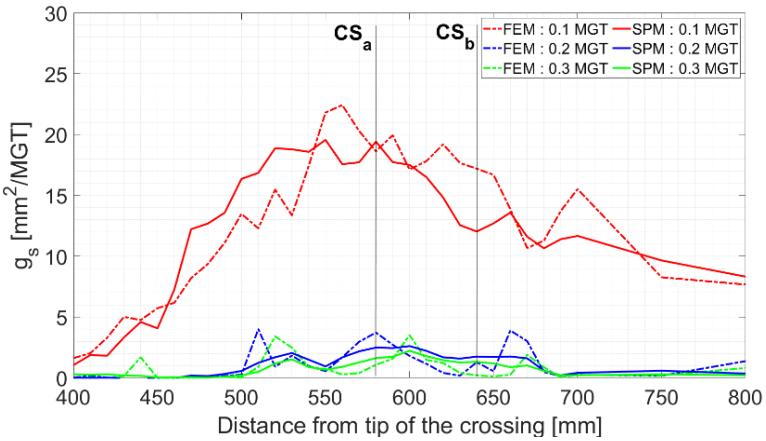


Figure 5: Comparative analysis of the FEM and SPM model results based on the rail profile shape change are calculation results. Plots show the correlation between the profile change area increments (ΔAs) from FEM (dotted line) / SPM (solid line) simulations.

Two chosen cross-sections were selected to represent a case for a good agreement between FEM results and the SPP model ($CS_a$) and one with a relatively high deviation ($CS_b$). The simulated profiles for both methods for these chosen cross-sections are shown in the **Fehler! Verweisquelle konnte nicht gefunden werden.**. For both cross-sections $CS_a$ and $CS_b$ the profiles show good qualitative and quantitative agreement: the maximum error is smaller than 0.5 mm$^2$. By adding additional features to the dependencies described in the Figure 4Figure 5 (e.g. consideration of the shear stresses in the contact patch) it might be possible to improve these results, which will a subject to further investigations.

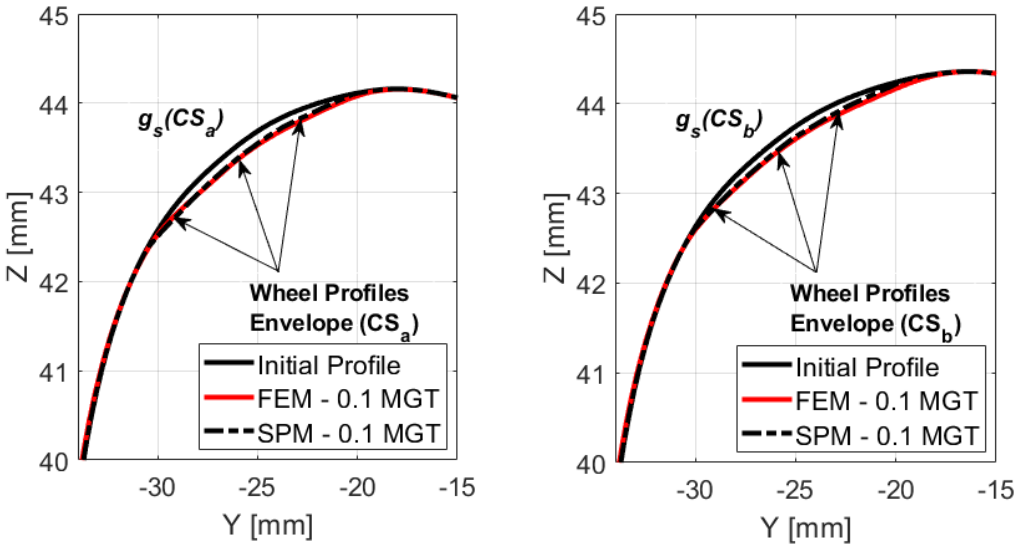


Figure 6: Rail profile evolution (FEM simulation results comparison with the SPP model simulation results for the two choosen cross-sections positioned along the turnout).

## 1.3 Conclusions

The developed SPP model simulation results are shown to be in good correlation with plasticity calculations carried out with FEM based approach for R350HT steel grade and confirmed our initial hypotheses for both shape change area development and profile shape prediction based on the accumulated effect of the wheel profiles. Due to the semi-physical nature of the model, the computational time for such predictions was observed to be significantly improved as compared to the analogous FEM-based models (order of minutes instead of weeks). The developed model can therefore be useful for the effective and time-efficient rail surface damage prediction using the MBD simulations as a basis for the rail plastic deformation prognosis in turnouts. Moreover, as a part of the whole system model framework, the developed SPP model is expected to contribute to the holistic track damage prognosis and can be used for example by turnout suppliers for the crossing nose design and material selection process improvement.

## 1.4 References

[1] K. Six *et al.*, "A whole system model framework to predict damage in turnouts," *Veh. Syst. Dyn.*, pp. 1–21, Oct. 2021, doi: 10.1080/00423114.2021.1988116.

[2] R. Skrypnyk, J. C. O. Nielsen, M. Ekh, and B. A. Pålsson, "Metamodelling of wheel–rail normal contact in railway crossings with elasto-plastic material behaviour," *Eng. Comput.*, vol. 35, no. 1, pp. 139–155, 2019, doi: 10.1007/s00366-018-0589-3.

[3] M. Pletz, K. A. Meyer, D. Künstner, S. Scheriau, and W. Daves, "Cyclic plastic deformation of rails in rolling/sliding contact –quasistatic FE calculations using different plasticity models," *Wear*, vol. 436–437, p. 202992, Oct. 2019, doi: 10.1016/j.wear.2019.202992.

[4] K. A. Meyer, R. Skrypnyk, and M. Pletz, "Efficient 3d finite element modeling of cyclic elasto-plastic rolling contact," *Tribol. Int.*, vol. 161, p. 107053, Sep. 2021, doi: 10.1016/J.TRIBOINT.2021.107053.

[5] U. Spangenberg, R. D. Fröhling, and P. S. Els, "Long-term wear and rolling contact fatigue behaviour of a conformal wheel profile designed for large radius curves," *Veh. Syst. Dyn.*, vol. 57, no. 1, pp. 44–63, 2019, doi: 10.1080/00423114.2018.1447677.

[6] Johansson et al., "Simulation of wheel-rail contact and damage in switches & crossings," Wear, 2011, doi: 10.1016/j.wear.2010.10.014.

[7] D. Niklitsch; J. Nielsen; M. Ekh; A. Johansson; B. Pålsson; A. Zoll, "Simulation of wheel–rail contact and subsequent material degradation in switches & crossings," *Proceedings 21st International Symposium on Dynamics of Vehicles on Roads and Tracks, Stockholm, Sweden, August 17-21, 2009, 14 pages (available on CD)*. https://research.chalmers.se/en/publication/108435 (accessed Jul. 20, 2022).

[8] L. Xin, V. L. Markine, and I. Y. Shevtsov, "Numerical procedure for fatigue life prediction for railway turnout crossings using explicit finite element approach," *Wear*, vol. 366–367, pp. 167–179, Nov. 2016, doi: 10.1016/J.WEAR.2016.04.016.

# 2 Rail Profile Prognosis Model and Crack Initiation Model

## 2.1 Hybrid profile evolution model

Profile wear and rolling contact fatigue (RCF) are some of the main contributors regarding service life of rails and are, thus, very important for maintenance planning. The goal of this work package was to develop a process that is able to perform the prediction of wear and RCF on a whole network. Therefore, not only accurate models are necessary, but also ones with a very low computational effort.

State of the art processes for profile wear prognosis are based on a plenty of multibody dynamic (MBD) simulations. The main problem of this method is that the diversity of the operational conditions leads to an exponential increase of the simulation effort. The main goal of this work package was to reach a good prediction quality with only a few representative MBD simulations.

For the presented approach, the so called "hybrid profile evolution model" was chosen [9]. This model was developed for wheels and needed to be modified to work for rails. The basis of this method is the assumption that a worn rail profile is mostly shaped by the passing wheel profiles and, after a given amount of time, will always wear similarly – assuming the same/similar wheel profile types. However, the time it takes for this change to happen will depend on different factors, e.g. materials, vehicle fleet, different axle loads, wheelset guiding stiffnesses, etc.

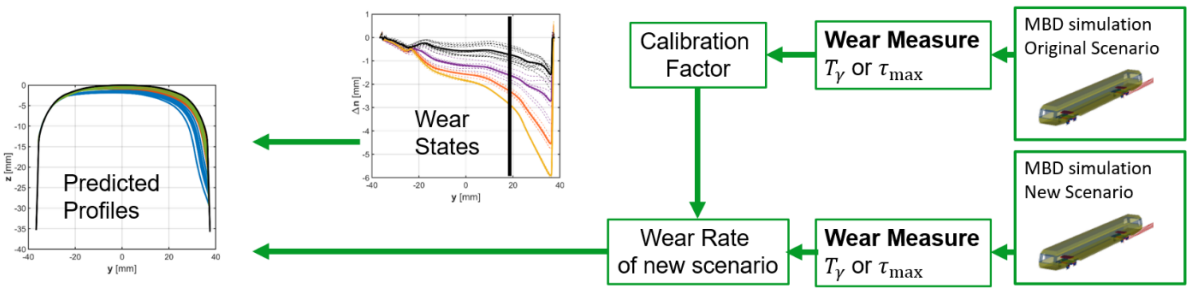


Figure 7: Concept of the wear prediction with the hybrid profile evolution model

If there are measured profiles available for a certain scenario (e.g. a certain curve radius) it is possible to use these directly for an analysis and the prediction of the resulting profiles. However, if there is a new scenario, where no profiles are available, it is possible to translate the results from the measurements to new scenarios.

In this so called hybrid approach, MBD results of the "Original scenario" (see Figure ) are used to derive a calibration factor. This factor is determined based on the measured wear volume. If the user wants to predict the wear for a new scenario (e.g. different curve radius or different cant), the according MBD simulations have to be carried out. If the vehicle fleet is different, it doesn't change anything on the MBD simulation effort, because it has an influence only on the weighting on the simulation results, on the so-called wear measures. These wear measures are either $T\gamma$ or $\tau_{max}$.

## 2.2 Application of the hybrid approach

The application of this methodology will be shown on a following validation exercise (see Figure ). First, the hybrid profile evolution model was validated for rails. Therefore, wear data from a curve with a radius R1 (blue dots) was used to calibrate the model, resulting in the blue continuous line in Figure 6. Then, the results were transferred by use of MBS-simulations to predict the black continuous line. This line fits very nicely to the measured wear on the second curve radius R2 (black dots).

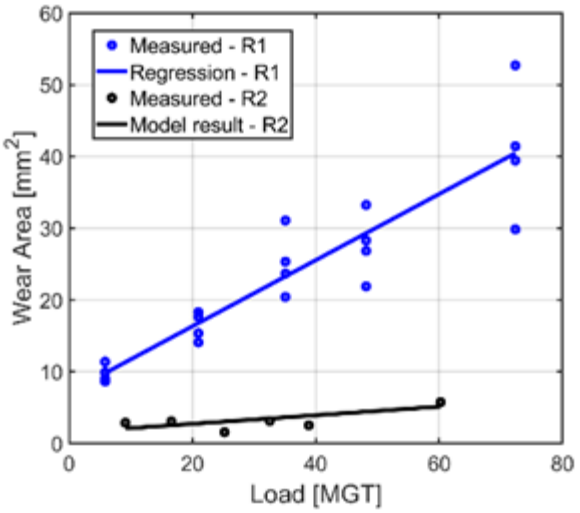


Figure 8: Measurement/Prediction comparison of the progress of wear area over the MGT.

This method can now be applied to all different scenarios as desired. Assuming known wear – measurement data – in two different curve radii, divided into rail head and gauge face wear (red crosses in Figure 9). Firstly, the calibration has to be carried out. For this step any available wear measurement can be used, even in a different network with different vehicle fleet in a different curve radius. It can be seen on the left-hand side figure, that a prediction over all of the curve radii with the calibration data gives a poor prediction quality

(blue lines) for both railhead (continuous) and gauge face (dashed line). If the results of the MBD simulation will be weighted according to the actual vehicle fleet, a good agreement can be reached. It has to be emphasized that if the vehicle types in the two different networks are the same but only the combination is different, no additional MBD simulation has to be carried out, only the weighting of the MBD results will be changed.

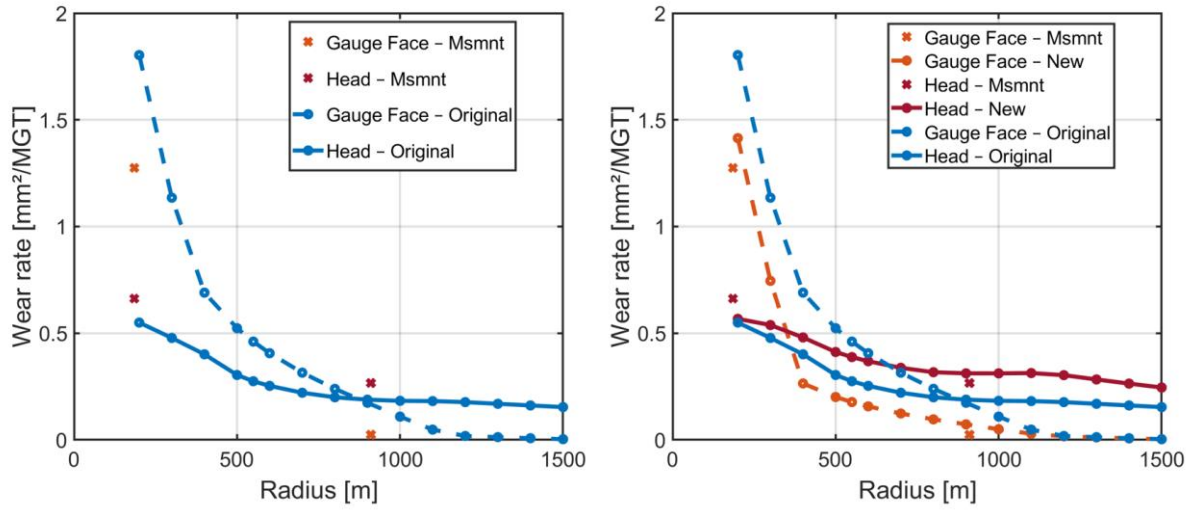


Figure 9: Prediction of the wear behavior over the curve radii on a part of the railway net based on measured wear on two radii (red crosses)

## 2.3 RCF prediction method

For the prediction of the crack initiation on rails, the so-called Wedge-model [10] was used. This is very time demanding and must be recalculated for every change in vehicle mix, which itself is rarely known.

In this work package a new approach has been developed to save computational time but keep the prediction quality as high as possible. So, the Wedge-model calculations have been carried out for each single vehicle type separately instead of a given vehicle mix directly. The results are then created by weighting the single vehicle results. Therefore, no additional computations are needed if the vehicle mix is changed.

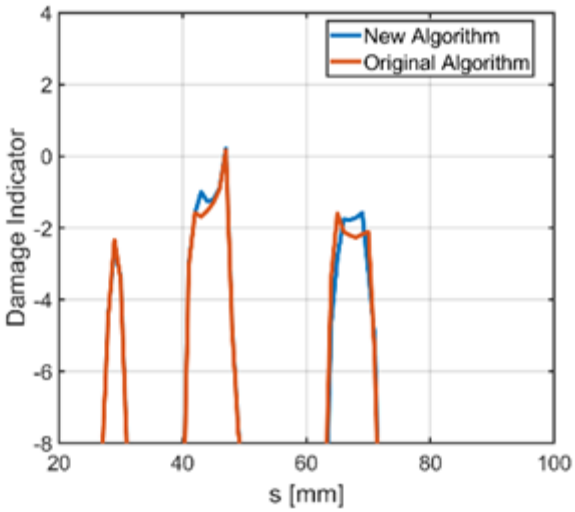


Figure 10: Damage indicator along the arc length of the rail profile (s).

In Figure , the red lines show the results of the original algorithm, were the MBS-simulation results were mixed before the crack initiation calculation.

The blue line shows the results for the new algorithm, where the crack initiation was computed for single vehicles and mixed afterwards. The damage indicators show a good correlation (see Figure ): both, the position of the maximum and the value itself is very similar. Thus, it is possible to change the vehicle mix without having to recalculate the crack initiation without a huge loss in quality of the prediction.

The analysis of the behaviour of the damage indicator has shown a nonlinear changing characteristic. After a fast change during the first cycles (see Figure 11) it seems to be became constant after 3-4 MGT's. It enables the possibility to calculate only the first 3-4 MGT's with this very time-consuming way and then extrapolate till the next available (measured) rail profile, which is usually at 10-15 MGT.

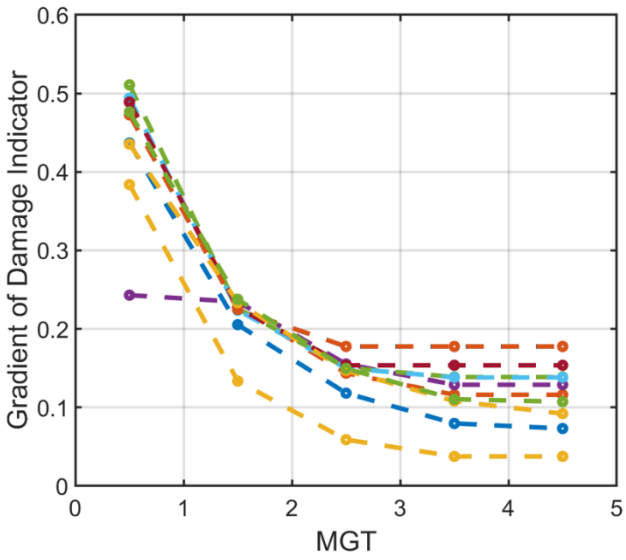


Figure 11: The change rate of the damage indicator depending on the load (MGT).

As it has been shown above, a fast and accurate methodology has been developed to predict the profile wear and the rail damage (RCF). The profile wear prediction algorithm can easily be applied to wheel profiles too, in this case the MBD simulations have to be carried out with the same vehicle model in different curve radii, according to the travelled line in the network.

The quality of the damage prediction can be increased due to the implementation of the measured wear into the process instead of a previously used wear law. In this case the amount of wear will be linearly interpolated in each calculation step.

## 2.4 References

[9] Hartwich, D., Müller, G., Meierhofer, A., Obadic, D., Rosenberger, M., Lewis, R., Six, K.: A new hybrid approach to predict worn wheel profile shapes, Vehicle System Dynamics, 2022

[10] Trummer, G., Marte, C., Dietmaier, P., Sommitsch, C.,Six, K.: Modeling surface rolling contact fatigue crack initiation taking severe plastic shear deformation into account. Wear, 2016

# 3 The multibody track model

## 3.1 Dynamic gauge widening - measurement and simulation

Particularly in mountainous regions, small curve radii are often necessary. The track systems there are heavily loaded by the high lateral forces in wheel-rail contact in these sections. This results in increased wear on both participants, the vehicle and the track. The smaller the curve radius, the more complicated the interactions between wheel and rail become.

This subproject of Area 2.1 focuses on the investigation of the dynamic gauge widening of curves with very small radii. The dynamic gauge widening is composed of the nominal gauge, the wear of the rail profiles and the temporary tilting of the individual rails, influenced by the dynamic force level and the position of the wheel-rail contact. The dynamic force level in a curve depends on other parameters, such as the alignment, the track components, the quality of the track, the bogie design, the vehicle speed and the environmental influences.

To investigate the various influencing variables, a multi-body simulation model was created at the Institute of Structural Durability and Railway Technology (BST) at Graz University of Technology. In the constructed track model, the left and right rails are modelled as rigid bodies connected to the sleeper by a spring-damper system. The ballast superstructure is also modelled by a spring and damper system. A representation of the track model and the vehicle model are given in Figure 12.

The stiffness parameters are determined by measuring the dynamic forces and the resulting deflection and are considered in the simulation.

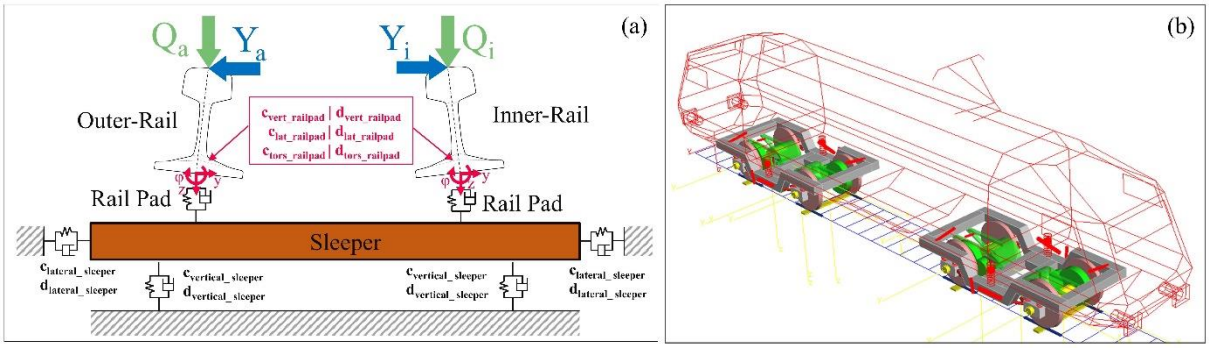


Figure 12: Schematic representation of the multibody track model (a) and the multibody model of the locomotive in SIMPACK (b)

This model allows not only the dynamic lateral displacement of the individual rails to be represented, but also their tilting. This allows the influence of rail pads with different stiffnesses on the vehicle-track interaction to be investigated. Simulation results show that the changes in contact geometry caused by rail tilting strongly depend on the specific wheel and rail profiles. This is illustrated by comparing a new rail profile with a worn rail profile. Special attention is also paid to the distinction of the dynamic track gauge between leading and trailing wheelsets. This depends, among other things, on speed, wear (wheel & rail) and unloaded track gauge. Due to the combination of contact position and vertical and lateral forces, dynamic track narrowing can also occur in trailing wheelsets.

Finally, the multi-body model was validated using measured wheel-rail forces and gauge widening in the track. For the measurement of the rail head movement, a measurement setup was developed by the Institute of Railway Infrastructure Design (RID) at Graz University of Technology and installed on one of the narrowest curves of the Austrian rail network. Several linear displacement sensors recorded the lateral rail head and rail foot movement. The measurements were carried out over several days under regular operation of different rail vehicles. The measurement setup is shown in Figure 13.

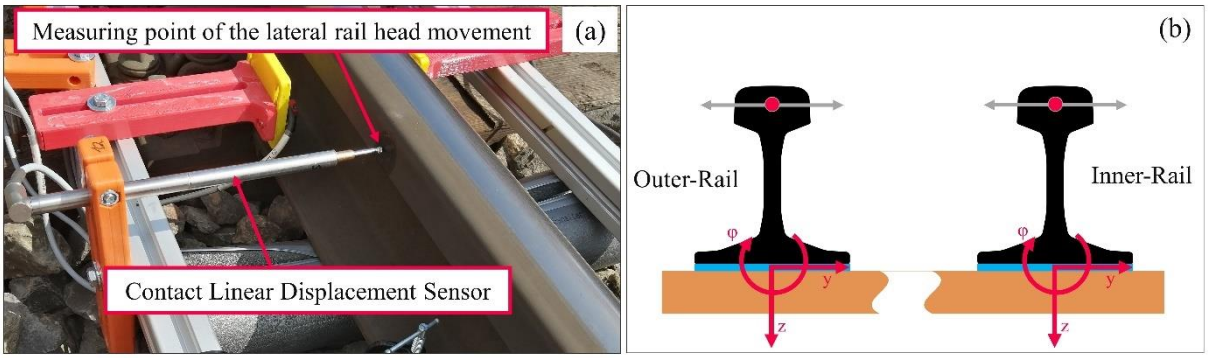


Figure 13: (a) Measurement setup for determining lateral rail head movement using linear displacement sensors, (b) Schematic and coordinate convention of the measurement setup

In order to record the influence of different curve radii and wear conditions of the rails, the measurements were carried out at three positions. The curve section was simulated in detail in the multi-body simulation. This includes all information of the alignment, but also measured rail profiles and stiffnesses of the superstructure. The speed profile of approx. 60km/h was measured and specified in the simulation. The comparison between measurement and simulation showed a good agreement in the different radii. The results are shown

in Figure . Here it can be seen that the inner and outer rails of the trailing wheelset tilt in the same direction towards the outside of the curve. Detailed investigations of the occurring interactions when passing through a narrow curve allow a better understanding of the dynamic gauge widening. The results of the validated simulation model provide a basis for further wear calculations by the project partners.

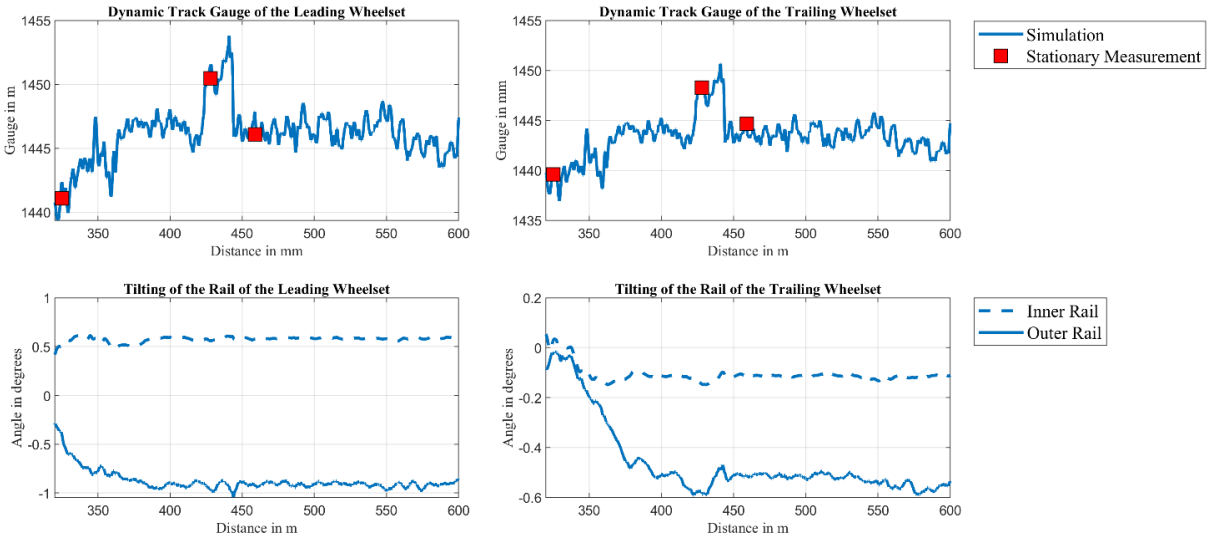


Figure 14: Comparison of dynamic track gauge and rail tilting in measurement and simulation

In the next step, the simulation model will be tested on another curve with a larger radius. Compared to the curve considered so far, this section contains concrete sleepers instead of wooden sleepers, and the larger radius of the curve means that the speed of the vehicles is also higher there.

The resulting digital twin will enable a time-dependent simulation of the behavior of the railway infrastructure under operational impacts and provides significant potential for the optimization of the holistic system.

## 3.2 Single failure development tool

The interaction between the rail vehicle and the railway track causes major loads in the overall rail system and can lead to high acquisition and maintenance costs. For this reason, the condition assessment of the track is of utmost importance for the railroad infrastructure company. If rapid deterioration of the track occurs at a singular point along the track, this is referred to as a single failure. Triggers are usually discontinuities in the track, such as bridge crossings. Many of them are recorded in a central database, which makes it easy to assign the cause of the change of track geometry. However, there are a large number of single failures whose cause is not categorized accordingly. These include rail joints, isolation joints, and culverts under the superstructure. Repeatedly passing over a rail joint, for example, often results in a track geometry failure that subsequently grows exponentially.

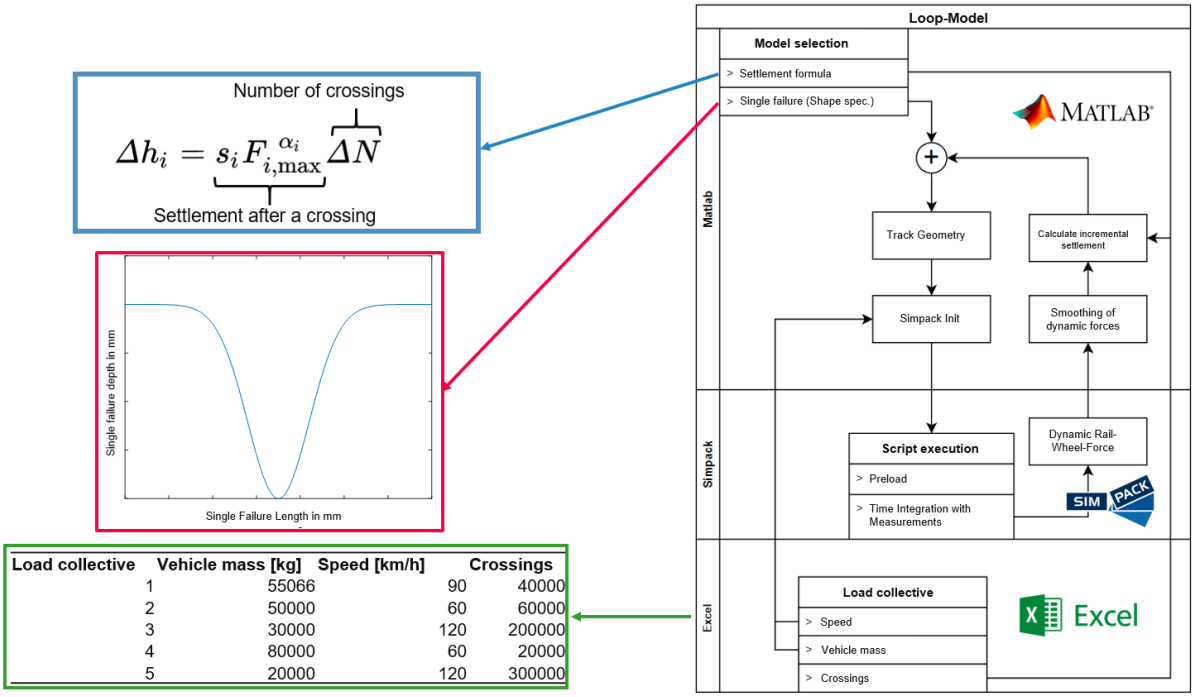


Figure 15: Process image for the simulation of single failure development

Since the geometric and also temporal development of single failures can be very different, various causes and their effect on the forces in the wheel-rail contact were investigated. For this purpose, simulations were carried out in a multi-body simulation program. Particular attention was paid to realistic modelling of the track system. A track model was built that allows the simulation of a geometric rail surface defect or a rapid change in track stiffness.

Now, in order to be able to simulate the prediction of track degradation over time, the multibody model was integrated into a looping process model, which can be seen in Figure 15. Given a geometric track surface defect, the multibody simulation provides the dynamic

wheel force. This is considered in an empirical settlement formula known from the literature. The settlement calculated from this after a specified number of crossings is then transferred back to the multibody model in the form of a new longitudinal level. This serves as the track system for the next iteration loop. In order to be able to represent the temporal development of a single failure, the mixed traffic operating in reality must also be modelled. For this purpose, a representative vehicle collective was defined. Subsequently, the simulation time could be reduced by determining the number of necessary loop runs on the basis of a parameter study.

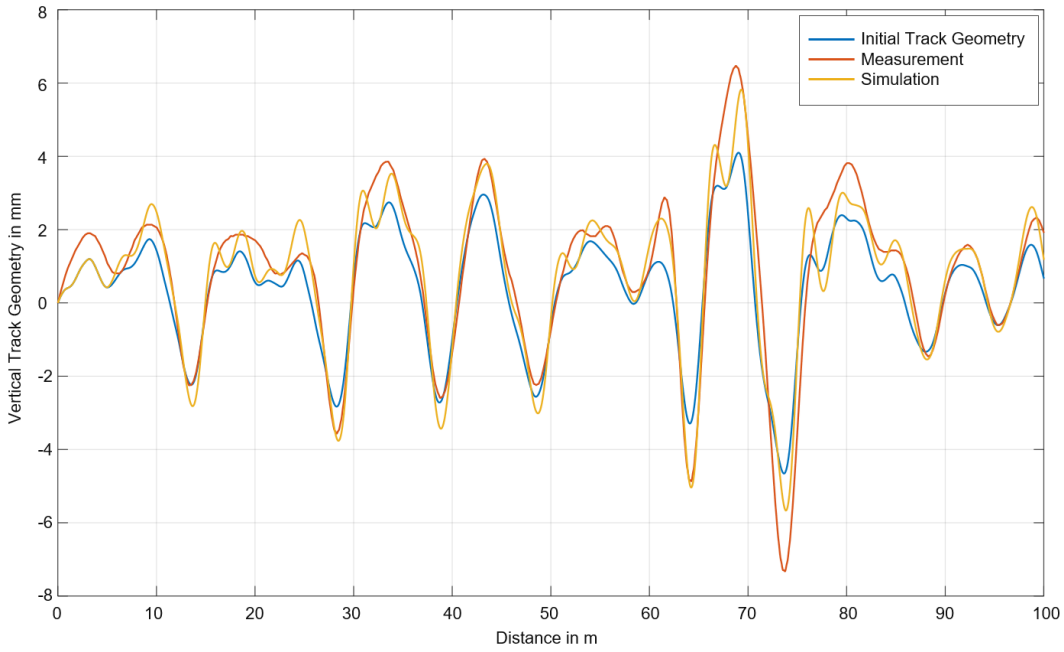


Figure 16: Validation of the single failure development tool on the basis of the track geometry measurement of a measuring section

Finally, the simulation model and the developed loop process model were validated using a short section of track with a single failure. Figure  shows the comparison of the simulation with the measurement, based on the initial track geometry measurement. For this purpose, a track-specific settlement factor was determined from existing track measurement data. On the basis of this, the further development of the single failure can be predicted. In addition to that the simulation offers the possibility of changing the vehicle mix, for example. Furthermore, basic parameters of the vehicle can also be changed virtually in order to investigate the effect on the track load. Thus, with the newly developed single failure development model, it is possible not only to derive an improved track geometry prediction for future track maintenance, but also to investigate the track-friendliness of vehicles and thus to further develop the overall rail system in a holistic manner [11].

## 3.3 Plausibility check of the rail surface signal for usage in multibody simulation

For the single failure development tool, the excitation of a multibody vehicle by short-wave defects of the rail surface was considered. The signal used there originates from a measurement of the measuring wagon of the Austrian Federal Railways (ÖBB), which runs regularly in Austria. A chord measurement method is used, which requires further post-processing of the data. The amplitude of the original measurement signal is distorted due to the special characteristics of this measurement method depending on the wavelength. A back-calculation algorithm was used which reproduces the original surface geometry with sufficient accuracy. To check the plausibility of this data processing, the measuring device RAILSTRAIGHT was used. This records the surface in the range of one meter and is normally used for quality control of welded joints. In the course of a measuring campaign, 20 rail joints were measured with the RAILSTRAIGHT and the results were compared with the measurements of the measuring wagon. The applicability of the processing algorithm was demonstrated and confirmed.

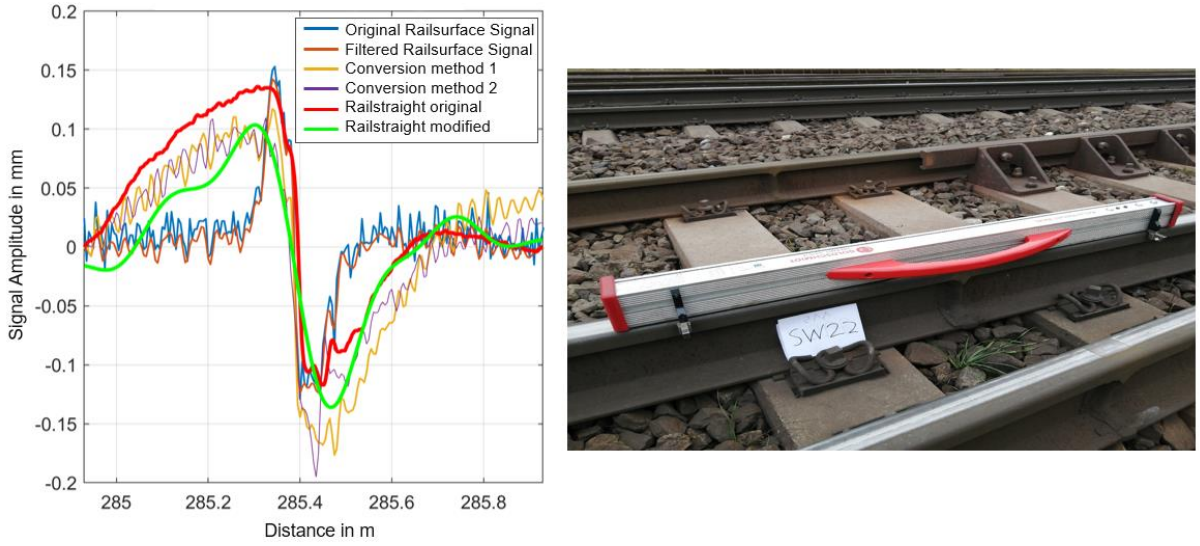


Figure 17: (a) Comparison of the mathematical processing of the rail surface geometry with the original signal and the measurement by means of the RAILSTRAIGHT measuring device (b)

Figure  shows an example of a welded joint. The original and the filtered rail surface signal (SOF) are shown. This processing step removes unrealistic peaks and reduces the computing time. Two different conversion methods were used, but it could be shown that their results do not differ. The conversion method according to [12] was applied. Finally, the RAILSTRAIGHT signal was presented in the same way in comparison. For a better comparability, the RAILSTRAIGHT signal and the SOF signal had to be brought to the same wavelength range. The representation shows a good agreement between the two signals. It was

thus shown that the processed rail surface signal can be used as excitation for the multi-body simulation.

## 3.4 References

[11] Großschädl Christopher. Aufbau eines Fahrweg-Einzelfehlerentwicklungsmodelles für die Mehrkörpersimulation von Schienenfahrzeugen [Masterarbeit]. Graz: Technische Universität Graz; 2023.

[12] Wolter KU. Rekonstruktion der originalen Gleislageabweichungen aus 3-Punkt-Signalen (Wandersehnenmessverfahren) und Beurteilung hinsichtlich Amplitude, Fehlerwellenlänge sowie Fehlerform. (EurailScienceEdition; vol. 4). Hamburg: Eurailpress DVV Media Group; 2012.

# 4 Influence of rail grinding on crack behaviour

Squats and squat-like defects are a very important issue for infrastructure provider. These defects are sometimes linked to residual roughness on the rail surface, especially after grinding.

## 4.1 Normal stress distribution

Rail grinding can, on the one hand, lead to white etching layers (WEL), which are mostly martensitic structures with high hardness and low ductility. It is believed, that these WEL can pose a risk to preliminary rail failure. For this reason, a 2D-FEM model was developed to investigate the influence of WEL on the contact stress between wheel and rail. The simulations showed that the presence of WEL in the contact zone led to stress raises on the interface between WEL and the surrounding bulk material, see Figure 18.

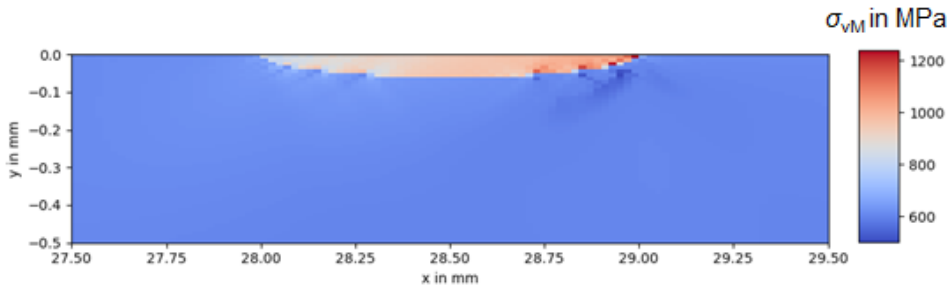


Figure 18: Maximum equivalent stresses at a semi-elliptical WEL

On the other hand, WEL are not the only influence on local contact pressure peaks. Another factor are the grinding grooves which are believed to have a significant influence on local pressure and stress distribution. The simulation of small geometric imperfections, such as grinding grooves cannot be efficiently modelled with FEM-Models, due to the necessity of very fine meshes and the modelling of the contact. To investigate the influence of grinding grooves, a normal contact model was developed, which allows a fine discretisation of the 3D-Contact geometry with geometric imperfections. The model is based on the boundary-element-method (BEM) for the contact of a rough surface with an elastic half-space.

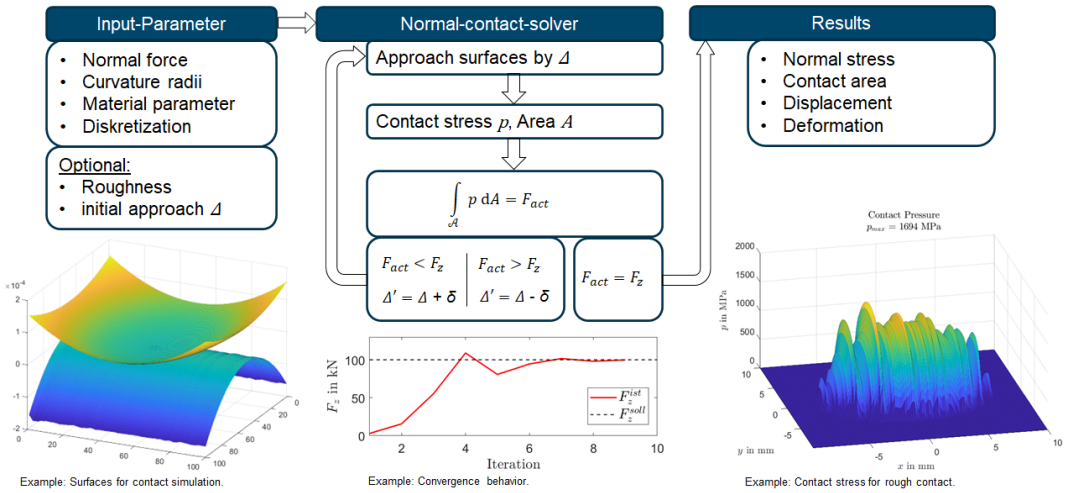


Figure 19: Working principle of the normal contact model.

This model (Figure 19) allows faster simulations of rough contact problems compared to the FEM. In a following step, the output from the contact model (pressure distribution on the rough surface) could be used as input for successive simulations with e.g., the FE-simulations or the DERC-Model to investigate the influence of rough surfaces on crack propagation.

## 4.2 The DERC-Model

The first step to investigate the crack growth was to use state of the Art FE-modelling. The results showed that the crack growth dependent heavily on the chosen crack growth model, sometimes leading to contradicting results.

Therefore, a different approach was chosen: For the macroscale model, a truss-like discrete element method (DEM) model was selected and optimised for the simulation of rolling contact fatigue (discrete element rolling contact, DERC model).

In the first step, an elastic parametrisation was performed to derive elastic stiffness' for the elements. The literature review did not provide a satisfying solution therefore. As a result, an optimisation method was developed to determine the elastic stiffness' for the three element types (longitudinal, vertical, diagonal). As a reference, the stresses for a specific sampling grid given by Johnson [13] were selected. This sampling grid was integrated to the DEM model (see Figure ). Therefore, stresses from the DEM grid were interpolated to give results for the sampling points. Then, the residuals were calculated for each sampling point by taking the squared difference of the equivalent Von Mises stresses. Finally, an optimisation was set up that varied the stiffness' to find

an optimum solution. In this way, the stress fields that result from Hertzian- or combined loads under the assumption of full sliding were modelled, see Figure .

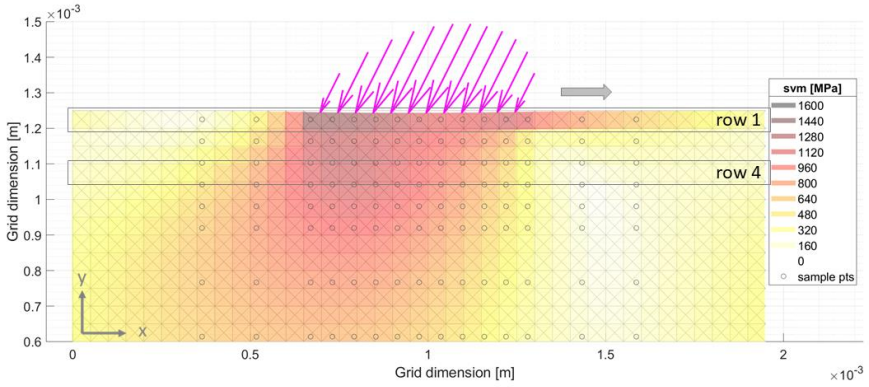


Figure 20: Equivalent stress field (Von Mises) under combined load for a twin disc test case, modelled by the truss-like DEM model. The sampling grid applied for the parametrisation is illustrated. The surface row and a subsurface row are marked.

In the next step, initial cracks were introduced. This was done by modifying the bond law of the selected elements, so that these failed elements ware capable of bearing compressive forces only. For the study, three surface cracks were introduced: One behind the rolling contact (traction case, crack #1), one in the centre (crack #2) and another one in front of the contact (crack #3), which is displayed in Figure 21. In this way, multiple cracks were introduced.

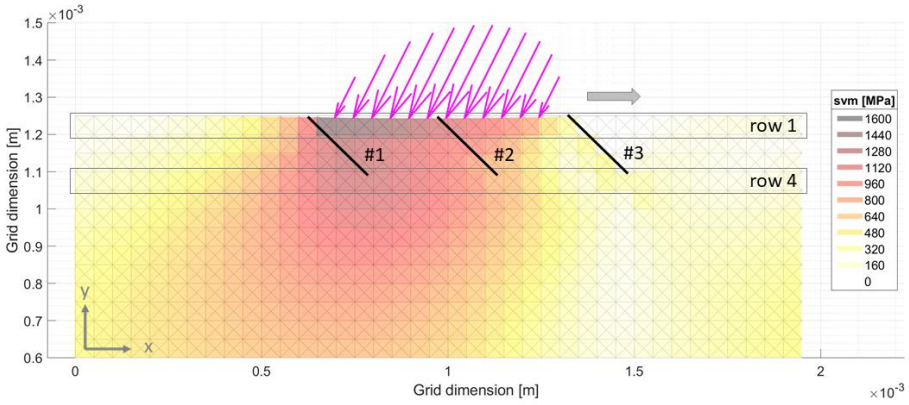


Figure 21: Rolling contact simulation and equivalent stress field for the case with three cracks.

Based on the simulation results, deviations of the stress fields (for normal stress in x direction, see Figure ) were compared to the undamaged case. The result is that stress peaks can be identified on crack tips under certain load conditions. This stress peaks are the potential driver for crack growth, which shall be modelled as a next step.

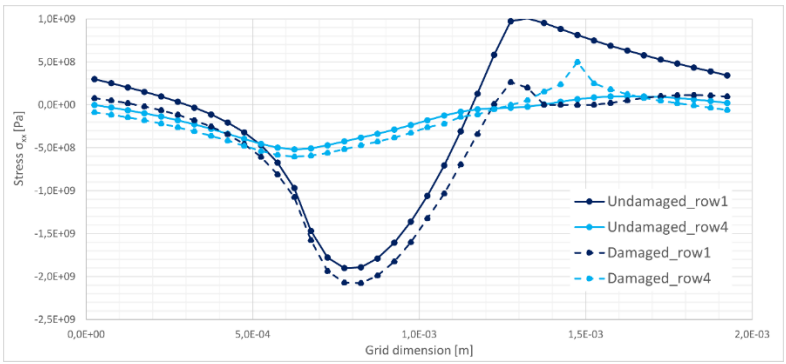


Figure 22: Analysis of the normal stresses in x-direction for the surface and subsurface rows. The undamaged and the damaged case are illustrated.

In the next step, a fatigue capability was defined by means of a fatigue law [14], which assigns each element a damage property called remaining life (see Figure ). The remaining life reduces per each load cycle as a result of the absolute element strain and two FCG parameters. It does not require an analysis of the stress intensity factor. In this way, the degradation as a result of multiple load cycles was modelled. The capability was evaluated for mode I and mode II cases, which delivered a satisfying agreement.

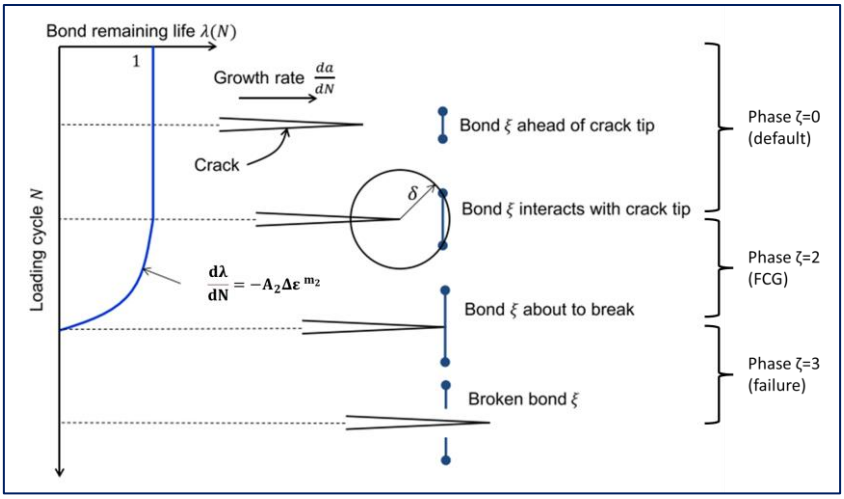


Figure 23: Principle of fatigue crack growth law (modified from Silling and Askari, 2014).

In the next step, the FCG capability was applied to simulate RCF. Therefore, an experimental reference of a full-scale test rig was adopted (see Figure 24). Isotropic FCG was assumed initially. Thus, the reference was selected with focus on FCG within an undeformed material to get a reference for isotropic FCG. An initial crack was introduced by cutting, then multiple load cycles were applied that resulted in a branching of two cracks around the initial crack tip.

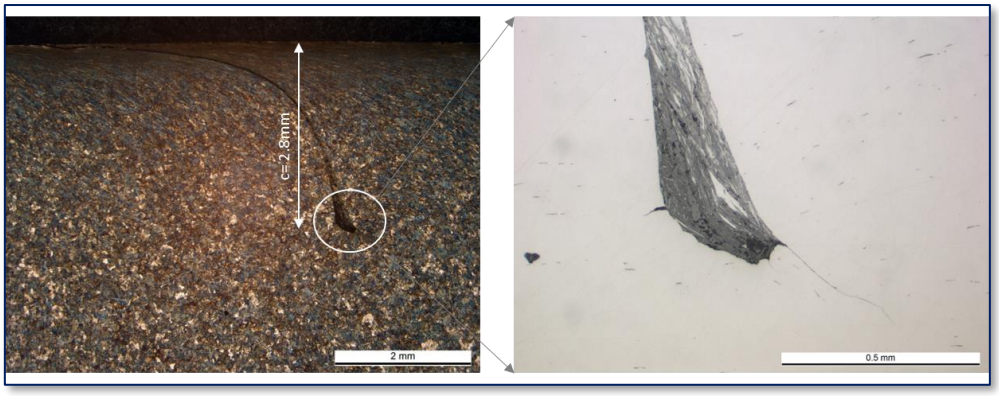


Figure 24: Metallographic sections of rig test [courtesy of voestalpine Rail Technology GmbH].

For the modelling, the configuration of the bond law is paramount, which defines the force response as a function of strain for healthy and failed elements. An initial bond law was used, where failed elements could still bear full compressive load, but no load in tension. The standard approach from the literature was additionally applied as default, where elements lose their entire capability to sustain loads. The RCF results indicated that the initial law did not lead to further crack growth at the tip of the initial crack. The result for the default bond law revealed a major shortcoming with regard to load propagation, as the completely soft crack could not transmit element forces anymore, which represented a kind of void. These results suggested that a bond law was required where failed elements bear a reduced stiffness.

Different set-ups of bond laws were developed and assessed as part of a parameter study. Based on that, a calibration with respect to crack closure was developed. With it, a bond law was derived that provided a reduced stiffness in compression with respect to

the initial approach. The novel bond law was integrated to the RCF simulation (see Figure 25), which was capable to reproduce the two branched cracks observed in the experimental study which is promising. Further, the branching capability was proven.

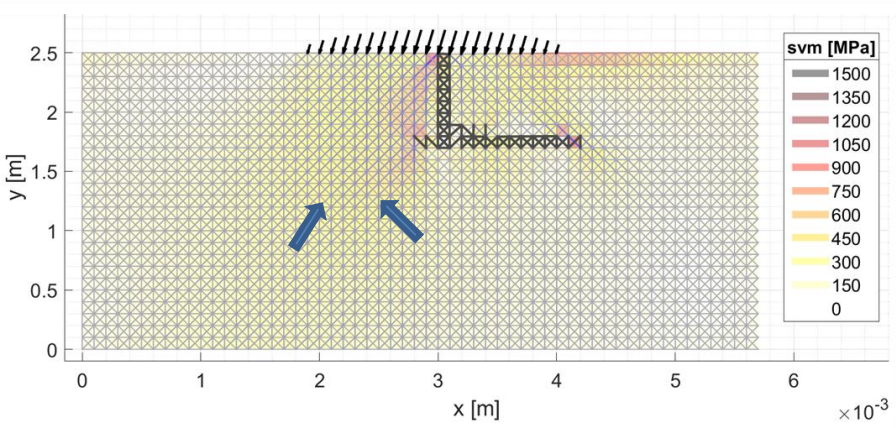


Figure 25: RCF simulation, where two cracks (red arrows) branch from the initial vertical crack.

A matter of further research regards the FCG pattern. A a better understanding of the grid's influence on the FCG development is required before the introduction of FCG anisotropy.

## 4.3 References

[13] Johnson KL, Contact Mechanics, First edit, Camebridge University Press; 1987

[14] Silling S, Askari; A peridynamic model for fatigue cracks, 2014; (SANDIA REPORT SAND 2014-18590), 1–39